

The Effect of Electrolyte and Additive Concentration on Zinc-Nickel Flow Cell Performance

David P. Trudgeon, Xiaohong Li*

*Renewable Energy Group, College of Engineering, Mathematics and Physical Sciences,
University of Exeter, Penryn Campus, Cornwall TR10 9FE, UK*

Abstract

This work aims to identify a suitable electrolyte composition for the operation of a zinc-nickel flow cell at ambient temperature. The effect of varying electrolyte composition containing KOH, ZnO, tetraethylammonium hydroxide (TEAH) or tetrabutylammonium bromide (TEAB) electrolyte additives are investigated. A 15 mM concentration of TEAH is found to provide smooth and compact zinc depositions. Increasing concentrations of KOH are found to be detrimental to voltaic efficiency, with coulombic efficiency peaking in 6 M KOH. The coulombic efficiencies of both zinc and nickel electrodes improve with ZnO concentration. Galvanostatic zinc-nickel flow cell cycling yields the highest efficiencies in an electrolyte of 6 M KOH with 0.5 M ZnO and 15 mM TEAH, with coulombic, voltaic and energy efficiencies of 98 %, 88 % and 86 % respectively over 70 stable charge/discharge cycles.

Keywords: Electrolyte additive; Zinc electrode; Zinc electrodeposition; Redox flow battery

* Corresponding author. *Email:* X.Li@exeter.ac.uk Tel: 0044 (0)1326 255769

1. Introduction

Redox flow batteries (RFB) represent one class of electrochemical energy storage system and have a number of advantages over other types of energy storage systems including mobility, flexibility, deep discharge, rapid response times, safe operation and large scale with power ratings from 10kW to 10MW. RFB technologies therefore constitute a promising solution for energy storage applications including grid services, such as load levelling, peak shaving and frequency regulation, and are also capable of facilitating implementation of renewable energy technologies by mitigating associated issues of intermittency and unpredictability [1–3].

Within the RFB family, the zinc-nickel redox flow battery (Zn-Ni RFB) possesses impressive key features over other RFB systems. For instance, the rapid kinetics of the redox couple provides a fast charge/discharge capability. The energy density of the system is large due to the relatively high standard thermodynamic cell potential of 1.73 V [4]. The Zn-Ni RFB system is seen to be cost competitive as it utilises inexpensive and abundant metals as active materials, and can employ only a single electrolyte with no requirement for membrane separators. This reduces the cost and design complexity of the system significantly [4–6]. For example, Turney *et al.* reported on a 25 kWh battery in 2014 with an estimated cost of just over 400 \$ kWh⁻¹ [5]. Additionally, the Zn-Ni system is environmentally friendly due to the use of low-toxicity zinc and nickel active materials. Despite this, challenges to implementation of the zinc-nickel RFB remain. On the one hand, system capacity is restricted by the amount of active material at the nickel positive electrode. To increase capacity, it needs to increase loading of active material of the electrode. On the other hand, the morphology of the zinc deposition at the negative electrode can be problematic. Dendritic or boulder morphologies can occur due to the inconsistent distribution of zinc deposition over

the surface area of the electrode, while H₂ and O₂ gas can evolve during charging at the zinc and nickel electrodes, respectively. This limits the system efficiency and durability [2,4,6,7].

There are a number of factors that can impact on the performance of the Zn-Ni RFB, in which, influential factors including electrode substrate materials [8–15], temperature [16,17], current density [17–22], electrolyte flow rate [21,22] are well reported. The use of additives to control zinc morphology has been extensively studied in zinc-based batteries and zinc electroplating [23–34]. However, literature concerning the effect of additives on Zn-Ni flow cells are less common [35,36]. Building on our previous work in which a total of 16 inorganic and organic additives have been systematically screened and discussed [36], in this work we examine the effect of two promising quaternary alkyl ammonium (QAA) additives, tetraethylammonium hydroxide (TEAH) and tetraethylammonium bromide (TEAB), on the performance of Zn-Ni RFB system.

Selection of electrolyte composition has significant impact on Zn-Ni RFB's performance. KOH or NaOH can be utilised as supporting electrolytes, but KOH is preferred due to its higher specific conductivity [37,38]. Previous studies of the effect of electrolyte composition (KOH and ZnO) on the rate of the parasitic hydrogen evolution reaction (HER), during zinc reduction, report that increasing KOH concentrations accelerate HER while increasing concentrations of Zn²⁺ suppress it [18,39]. Vaidyanathan *et al.* have observed that increasing concentrations of KOH lead to improved nickel electrode discharge capacities [40]. In addition, Chen *et al.* report that both discharge capacities and potentials of the nickel electrode increase with Zn²⁺ content, attributing this to the stabilising effect of the intercalation of Zn²⁺ ions to the nickel hydroxide lattice [41].

This research work focuses on the identification of a suitable electrolyte composition in terms of KOH, Zn²⁺ and additive concentration for use in the Zn-Ni RFB at ambient temperature (293 K). The QAA electrolyte additives TEAH and TEAB are assessed across a

range of concentrations in terms of their effect on zinc morphology and zinc electrode performance. Thereafter, a range of electrolyte compositions (KOH and ZnO) is investigated in relation to their effect on both the zinc and nickel electrodes individually and the full cell performance.

2. Experimental

2.1 Electrolyte chemicals

The base electrolyte consisted of KOH (Acros Organics, analytical grade, 85 %) and ZnO (Fisher Chemical, AR grade, 99.5+ %). The electrolyte additives were tetraethylammonium bromide (Sigma-Aldrich, reagent grade, 98%) and tetraethylammonium hydroxide (Sigma-Aldrich, 20 % wt. in H₂O). All chemicals were used as received.

2.2 Electrode materials and preparation

The nickel electrode material consisted of a commercial sintered nickel plate (Jiansu Highstar Battery Manufacturing Co. Ltd.). For utilisation in the zinc-nickel flow cell, this was prepared by cutting into segments of 2 cm × 2 cm which were washed with deionised water and allowed to dry prior to use. For cyclic voltammetry, this was cut into segments of 1.5 cm × 5 cm and masked to expose an area of 0.25 cm² (0.5 cm × 0.5 cm) using polypropylene tape with an acrylic adhesive (Avon tapes, AVN9811060K, 25 μm thickness) before a final rinse with deionised water prior to use. The zinc electrode substrate was a graphite polymer composite (Eisenhuth, BMA5 graphite/polyvinylidene fluoride). This was prepared in the same manner as the sintered nickel, with the addition of a polishing phase using emery paper (Simply Brands, Wet and Dry Paper, 3000 grit) prior to masking and rinsing the electrode. The Hg/HgO reference electrode was prepared in a 6 M KOH solution using the following chemicals; mercury (Acros Organics, 99.999 % metals basis), mercury (II) oxide (Acros

Organics, 99+ %). For three electrode half-cell experimentation a platinum mesh counter electrode (Alfa Aesar, 99.9 % metals basis) was employed.

2.3 Electrolyte properties

Conductivity, viscosity and density measurements of electrolytes with different KOH and ZnO concentrations were taken at 293 K. Conductivities were obtained using a Jenway 4330 conductivity meter. Kinematic viscosities were measured using an SI analytics 516 13 micro-Ostwald viscometer, with five measurements made for each electrolyte and the average taken. Measurement error was found to be within +/- 2%. Densities were obtained by weighing 1 mL of solution on a mass balance, and dynamic viscosities calculated using the measured densities and obtained values for kinematic viscosity.

2.4 Electrochemical methods

Electrochemical measurements were taken using a BioLogic SP-300 potentiostat and EC-Lab software at room temperature (293 K). Cyclic voltammetry and chronoamperometry were carried out in a 20 mL three electrode half-cell utilising a commercial sintered nickel electrode or graphite/PVDF composite as the zinc electrode substrate, prepared as described in section 2.2. Cyclic voltammograms were obtained at potential scan rates of 10 or 20 mV s⁻¹ over 25 cycles. For chronoamperometry in the zinc half-cell the working electrode potential was held at -1.6 V vs. Hg/HgO for a period of 1 hour.

Zinc-nickel flow cell cycling tests were conducted using a C-Flow laboratory cell (C-Tech Innovation, 1 cm × 1 cm working electrode area, 1.2 cm electrode gap). A peristaltic pump (Watson-Marlow 323S) and Marprene tubing (Watson Marlow, 3.2 mm I.D., 6.4 mm O.D.) were employed to pump 100 ml of the electrolyte solutions through the cell at a volumetric flow rate of 360 mL min⁻¹, providing an average linear velocity in the cell of 5 cm s⁻¹. Galvanostatic cycling tests were carried out at charge current densities of 20 mA cm⁻² to a capacity of 3 mA h and discharged at the same current density to a cut off cell potential of 0.8

V. Electrodepositions of zinc were obtained from the flow cell at the end of galvanostatic cycling tests by application of a final charge phase at 20 mA cm^{-2} to 3 mA h capacity. The surface morphology of these samples was characterised using a FEI Quanta FEG 650 SEM, operated at an accelerating voltage of 5 kV and a working distance of 5 mm.

3. Results and discussion

3.1 Effect of TEAH and TEAB additives

3.1.1 Cyclic voltammetry

Fig. 1a and 1b present the cyclic voltammograms of zinc deposition and dissolution recorded in electrolyte solutions containing additives at various concentrations ((a) TEAH, (b) TEAB). The resultant zinc deposition (reduction) onset potentials, E_R , anodic/cathodic peak separations, ΔE_p , and anodic/cathodic charge ratios are provided in **Table 1**. It can be seen that E_R shifted negatively with increasing concentrations of both TEAH and TEAB additives. While the inclusion of 1 mM of either additive has little effect, the inclusion of 20 mM causes negative shifts in E_R of 30 mV for TEAH and 48 mV for TEAB respectively. This trend can be explained by adsorption mechanism of the additives previously reported [26,29,36]. Increased concentrations of the additives lead to higher adsorption of the additive to the electrode, producing an inhibition effect and thus larger zinc reduction overpotentials. On the other hand, zinc oxidation is also inhibited by increasing additions of both TEAH and TEAB, with concentrations of 5 mM and above producing a positive shift in anodic peaks as shown in **Fig. 1a and 1b**. The anodic/cathodic peak separation increases with additive concentration, from 205 mV with no additive to 267 mV with 20 mM in the case of both TEAH and TEAB. This polarisation of zinc reduction and oxidation potentials with increasing additive concentrations results in reduced voltaic efficiency during full cell charge/discharge cycling, as reported in section 3.1.3.

As shown in **Table 1**, the value of anodic/cathodic charge ratios increase with additive concentration. With no additive the charge ratio is 0.82, and this increases considerably to 0.96 with 15 mM inclusions of both TEAH and TEAB additives. However, further increasing the additive concentration to 20 mM does not cause a significant change in charge ratios. This indicates that improvements to full cell charge/discharge cycling coulombic efficiency may be achieved with either additive at concentrations up to 15 mM, but no further gains beyond this concentration are likely.

3.1.2 Chronoamperometry and Chronocoulometry

Fig. 2a and **2b** provide the results of chronoamperometry obtained during zinc reduction. A potential of -1.6 V vs. Hg/HgO was applied for 1 hour with TEAH and TEAB additives at varying concentrations with the resultant current ranges displayed in **Table 1**. As shown, the current range becomes smaller with increasing additive concentrations. With no additive the current range is 201 mA, and this reduces with increasing additions of both TEAH and TEAB additives. The responses are very similar at 15 mM concentrations of both additives, providing current ranges of 62 mA. The smallest current range of 43 mA results from the addition of 20 mM TEAH. This is in a good agreement with previous studies by Wilcox and Mitchell [26] and Lan *et al.* [29]. They reported that increasing additive concentrations increase the efficacy of zinc dendrite suppression, consequently reducing the surface area of electrodeposited zinc, resulting in lower current ranges.

In order to provide estimates of the active surface area of zinc deposits obtained by chronoamperometry in the presence of varying additive concentrations, Anson plots are applied for a period of 10 seconds on zinc depositions obtained at a constant potential of -1.6 V vs. Hg/HgO until the charge passed reached 36 C (10 mA h) as illustrated in **Fig. 2c** and **2d**. The Anson equation (1) is provided below, where Q is charge passed, n is the number of

electrons involved in the reaction, F is the Faraday constant (96486 C mol^{-1}), C_0 is the initial concentration of Zn(OH)_4^{2-} in mol cm^{-3} , t is the time in seconds, A is the electrochemically active surface area of the electrode in cm^2 and D is the diffusion coefficient of Zn(OH)_4^{2-} in 6 M KOH at room temperature [42]. D has been determined experimentally as $2.25 \times 10^{-6} \text{ cm}^2 \text{ s}^{-1}$ as detailed in the supplementary information.

$$Q = \frac{2nFAC_0D^{0.5}t^{0.5}}{\pi^{0.5}} \quad (1)$$

By application of the Anson equation to the plots of Q vs. $t^{0.5}$ as shown in **Fig. 2c** and **2d**, the active surface areas of the zinc deposits have been calculated and are presented in **Table 1** along with the coefficients of determination in each case. Coefficients of determination between 0.983 and 0.993 have been obtained and the estimated active surface areas demonstrate the expected trend. With no additive, the estimated surface area of the zinc sample is 25.7 cm^2 . This reduces as the concentration of either TEAH or TEAB additive increases, to a minimum of 15.9 cm^2 with 15 mM of additive in both cases. With TEAH and TEAB in 20 mM concentrations, however, the estimated active surface areas rise marginally to 16.7 cm^2 and 16.3 cm^2 respectively, indicating a possible deterioration of the additives' ability to control zinc morphology at this concentration. This is corroborated by the results of SEM in section 3.1.3.

3.1.3 Zinc-nickel flow cell cycling

Fig. 3 reports the coulombic efficiencies for a zinc-nickel flow cell with TEAH and TEAB additives. Average efficiencies and electrode potentials are given in **Table 2**. In many cases the performance of the cell rapidly becomes erratic with fluctuating coulombic efficiencies. 80 charge/discharge cycles were completed in all cases. In **Fig. 3**, however, coulombic efficiencies are reported only to the point that erratic performance commences in order to maintain clarity of the figure. **Fig. 4** provides the individual electrode potential

responses for the first 30 charge/discharge cycles in the case of no additive, demonstrating the cause of the observed deterioration in coulombic efficiency. Over the initial 10 cycles, the poor coulombic efficiency of the cell (the black curve in **Fig. 3**) is due to limited discharge capacity of the nickel electrode (**Fig. 4a**). During subsequent cycles, as the discharge capacity of the nickel electrode increases, the coulombic efficiency of the cell becomes dependent on the discharge capacity of the zinc electrode, as shown in **Fig. 4b**, the erratic nature of this being caused by boulder type zinc morphologies, as evidenced by the results of SEM discussed below.

Table 2 shows that the voltaic efficiency of the zinc-nickel flow cell is attenuated as the concentration of either TEAH or TEAB increases. With no additive, the average voltaic efficiency approaches 90 %, but this decreases to under 89 % with the inclusion of either additive at 5 mM concentration. At additive concentrations of 10 mM and 15 mM, voltaic efficiencies are around 88 %. The lowest voltaic efficiencies are observed with the highest additive concentration of 20 mM, at 87.3 % with TEAH and 87.6 % with TEAB.

As shown in **Table 2**, the average electrode potentials demonstrate that the attenuation of voltaic efficiency is caused by the increase of zinc electrode polarisation with increasing additive concentrations, as expected following the results of cyclic voltammetry discussed in section 3.1.1. For example, with no additive the average zinc reduction/oxidation polarisation is 50 mV, increasing to 65 mV in the presence of 5 mM of either additive, around 80 mV with 10 mM concentrations, 90 mV with 15 mM, and 100 mV at 20 mM, respectively. This trend is due firstly to the inhibition effect of the additives observed in section 3.1.1 [26,29,36], and secondly the reduced electrochemically active surface area of zinc electrode modified by the additives. On the other hand, the average potential of nickel electrode remains unaffected by TEAH or TEAB additives with the average charge/discharge polarisation varying by no more than 4 mV.

Fig. 5 illustrates the SEM images of zinc morphology, which is directly linked to cell performance. As shown in **Fig. 5a**, with no additive present, zinc morphology is irregular and consists of clusters of small boulder type structures. Corresponding coulombic efficiency is low, at 95.2 %, and becomes erratic after only 20 cycles. The addition of 5 mM TEAH improves coulombic efficiency to 96 % and the zinc deposit is largely smooth and compact with some remaining areas of porous morphology (**Fig. 5b**). At 10 mM predominantly smooth and compact zinc depositions are obtained (**Fig. 5c**), and coulombic efficiencies approach 97 %. Stable performance is achieved over longer period but degrades after around 50 cycles. The highest coulombic efficiency of 97.8 % is achieved with a 15 mM concentration of TEAH, and performance is stable over 80 charge/discharge cycles. The corresponding zinc morphology is almost completely compact, as shown in **Fig. 5d**. When additive concentrations reach 20 mM the quality of zinc morphology diminishes, with large boulder structures occurring in a few locations on the electrode (**Fig. 5e**). In this case the cell fails after 15 cycles, continued cycling producing inconsistent performance and a significantly reduced average coulombic efficiency of 89.2 %. This is thought to be due to excessive adsorption of the additives to the electrode at this concentration, as represented in **Fig. 6**. TEAH and TEAB electrolyte additives function by specific adsorption of the cationic tetraethyl alkyl groups to zinc protrusions during electrodeposition, suppressing or preventing further zinc deposition in these locations. This promotes zinc reduction on other areas of the electrode resulting in a levelling effect and producing smoother and more compact zinc morphology[29,43]. In the case of an effective or moderate concentration (**Fig. 6a**) the growth of protrusions of zinc at the electrode are effectively suppressed, leading to a levelling effect and compact zinc depositions, as shown in **Fig. 5d**. However, in the presence of an excessive concentration of additive (**Fig. 6b**) adsorption occurs not only at zinc protrusions but also at other areas of the electrode leaving a significantly reduced area available for

further zinc deposition. The remaining areas are therefore exposed to increased current densities and increased diffusion limitations to zinc reduction, resulting in the formation of boulder type morphologies as observed in **Fig. 5e**.

In summary, 15 mM TEAH has been selected as the optimal additive concentration for further study as this displays the highest average coulombic efficiency of 97.8 %, high average energy efficiency of 86 % and the most stable performance over 80 charge/discharge cycles. SEM characterisation of zinc deposits at the end of cycling tests also show that the most improved morphology occurs with TEAH at a 15 mM concentration.

3.2 Effect of Electrolyte concentration

3.2.1 Properties of electrolyte solutions

The viscosity and conductivity of solutions, containing KOH in concentrations between 4 M and 8 M and ZnO concentrations between 0.3M and 0.7 M, have been obtained and are provided in **Table 3**. The highest conductivity of 501 mS cm⁻¹ is obtained in 6 M KOH solution containing 0.3 M ZnO and 15 mM TEAH in agreement with previous work confirming that KOH conductivity peaks at around 6 M at 293 K [37,44,45]. A 6 M KOH solution containing no ZnO demonstrated a conductivity of 561 mS cm⁻¹, in close agreement with previously reported values [44]. As shown in **Table 3**, the addition of ZnO decreases the conductivity of the solution, which is attributed to K⁺ and Zn(OH)₄²⁻ forming neutral associated ion pairs [46]. The relationship between conductivity and ZnO concentration has been shown to be a linear relationship as shown by equation (2) where κ is the conductivity, a is the solution conductivity with no ZnO addition, b is the slope of the regression line and C_o is the ZnO concentration [46,47].

$$\kappa = a - b \cdot C_o \quad (2)$$

Analysis of the results in **Table 3** yields values of b of -73 and -197 $\text{mS mol}^{-1} \text{L}^{-1} \text{ZnO}$ for 6 M and 8M KOH respectively. **Table 3** shows that the dynamic viscosity of the solutions increases with KOH concentration, from 1.782 mPa s^{-1} in 4 M KOH/0.3 M ZnO to 3.231 mPa s^{-1} in 8 M KOH/0.3 M ZnO. The addition of ZnO also increases viscosity, as previously reported by Siu and Evans [48].

3.2.2 Potassium hydroxide concentration

Fig. 7 provides cyclic voltammograms at zinc and nickel electrodes in electrolytes containing 0.3 M ZnO and KOH in concentrations between 4 M and 8 M. For the deposition/dissolution of metals, the point at which the voltammogram intersects the potential axis on the positive scan, ($E_{j=0}$), provides a reliable estimate of the equilibrium potential of the redox couple [49]. For the nickel electrode, the potential at which current density is zero on the positive scan, $E_{j=0}$, has been used to demonstrate the potential shift in differing KOH concentrations, and the results provided in **Table 3**.

For both electrodes, a negative shift is observed with increasing KOH concentration. In solutions containing 0.3 M ZnO, $E_{j=0}$ for the zinc electrode is -1.354 V vs. Hg/HgO in 4 M KOH and is shifted by -44 mV in 6 M KOH and a further -13 mV in 8 M KOH to -1.411 V vs. Hg/HgO (**Fig. 7a, Table 3**). This trend is in agreement with the equilibrium potentials observed by Bockris *et al.* and Hendrikx *et al* [50,51]. For the nickel electrode the same negative shift is observed, with an $E_{j=0}$ of 0.307 V vs. Hg/HgO in 4 M KOH being shifted to 0.284 V vs. Hg/HgO in 6 M KOH and 0.251 V vs. Hg/HgO in 8 M KOH, a total change of -56 mV (**Fig. 7b, Table 3**).

At the zinc electrode, reduction overpotentials increase significantly with KOH concentration. Overpotentials at -30 mA cm^{-2} , taken from the cyclic voltammograms shown

in **Fig. 7a** and **Table 3**, increase from -58 mV in 4 M KOH to -92 mV in 6 M KOH and -129 mV in 8 M KOH. This is due to two factors; firstly, the increasing electrolyte viscosity with KOH concentration restricts the mass transport of Zn^{2+} species to the electrode, resulting in larger concentration polarisation and, secondly, the enlargement of nucleation loops with KOH concentration observed in **Fig. 7a** due to nuclei with low volume and high surface area being readily oxidised [52]. In the case of zinc, the initial rate of oxidation has been shown to increase with KOH concentration [53]. It is therefore to be expected that formed zinc nuclei are more easily dissolved in electrolytes containing higher concentrations of KOH, resulting in the requirement for larger nucleation overpotentials to form stable nuclei and coherent zinc deposits [54].

Zinc oxidation overpotentials at 30 mA cm^{-2} have been taken as the difference between the potential at which current density reaches 30 mA cm^{-2} on the positive scan of voltammograms reported as shown in **Fig. 7a** and the corresponding values of $E_{j=0}$ in Table 3. These are relatively unaffected by KOH concentration, but do diminish from 44 mV in 4 M KOH to 39 mV in 6 M KOH and 36 mV in 8 M KOH due to the increased availability of OH^- at the electrode. Typical charge/discharge potential plots for the zinc electrode during zinc-nickel flow cell cycling given in **Fig. 7c** also demonstrate this trend. The charge/discharge polarisation increases from 76 mV in 4 M KOH to 103 mV and 145 mV in 6 M and 8 M KOH respectively, this being predominantly caused by increasingly negative zinc reduction potentials. In terms of the zinc electrode, increasing KOH concentrations therefore have a negative effect on voltaic efficiency.

At the nickel electrode the inverse is true, as shown in **Fig. 7b**. Oxidation overpotentials at 100 mA cm^{-2} decrease from 259 mV to 191 mV and 168 mV in 4 M, 6 M and 8 M KOH respectively, due to the increased availability of OH^- at the electrode. Reduction overpotentials also diminish as KOH concentration increases, although to a lesser extent,

resulting in nickel electrode polarisations of 415 mV, 328 mV and 302 mV at +/- 100 mA cm⁻² in 4 M, 6 M and 8 M KOH respectively. This trend is again observed during zinc-nickel flow cell cycling, as shown in **Fig. 7d**, with the nickel electrode charge/discharge polarisation of 199 mV in 4 M KOH decreasing to 186 mV in 8 M KOH. While this may be expected to have a positive effect on voltaic efficiency, it is insufficient to offset the negative effect on the zinc electrode. Increasing KOH concentrations are therefore detrimental to voltaic efficiency during zinc-nickel flow cell cycling, which reduces from 85.3 % in 4 M KOH to 85.1 % in 6 M KOH and 83.3 % in 8 M KOH. During zinc-nickel flow cell cycling, the coulombic efficiency is limited by the discharge potential of the nickel electrode in all cases, as shown in **Fig. 7d**, and follows the same trend observed from Q_c/Q_a during cyclic voltammetry. The highest coulombic efficiency of 97.5 % is achieved in 6 M KOH, reducing to around 93% in 4 M and 8 M KOH (**Table 3**). The improvement between 4 M and 6 M KOH is attributed to increased conductivity and availability of OH⁻ at the electrode, while the higher viscosity and lower conductivity of 8 M KOH accounts for the subsequent deterioration of performance.

3.2.3 Zinc oxide concentration

Cyclic voltammograms for the zinc electrode obtained in electrolytes containing varying concentrations of ZnO are displayed in **Fig. 8a**. As the rate of zinc reduction is proportional to the concentration of Zn²⁺ at the electrode [50,51] it is to be expected that higher ZnO electrolyte concentrations will result in increased reduction rates. This can be observed by the overpotentials at -30 mA cm⁻². The overpotential with 0.3 M ZnO is -129 mV, reducing to -126 mV and -122 mV in 0.5 M and 0.7 M ZnO, respectively. Zinc oxidation overpotentials are relatively unaffected by ZnO concentration since the rate of zinc

oxidation is independent of Zn(OH)_4^{2-} concentration at the electrode. The resultant zinc electrode charge/discharge polarisation reduces as ZnO concentration increases. At +/- 30 mA cm^{-2} during cyclic voltammetry this is 165 mV in 0.3 M ZnO, 161 mV in 0.5 M ZnO and 153 mV in 0.7 M ZnO, while during galvanostatic zinc-nickel flow cell cycling at +/- 20 mA cm^{-2} average zinc electrode polarisations are 145 mV, 135 mV and 131 mV across the same ZnO concentration range. Increasing ZnO content in the electrolyte may therefore be expected to be beneficial for voltaic efficiency in the zinc-nickel flow cell.

However, as shown in **Fig. 8b**, the polarisation of the nickel electrode increases with ZnO concentration. During cyclic voltammetry at +/- 100 mA cm^{-2} these are 302 mV, 325 mV and 357 mV in 0.3 M, 0.5 M and 0.7 M ZnO, respectively. This translates to average nickel electrode charge/discharge polarisations of 186 mV, 194 mV and 197 mV during zinc-nickel flow cell cycling (**Fig 7d**), which offsets the reduction in zinc electrode polarisation across the same ZnO concentration range. The resultant voltaic efficiencies therefore remain largely constant at around 83 %.

Coulombic efficiency of both electrodes is improved by increasing ZnO concentrations in the electrolyte. Zinc electrode charge ratios, Q_a/Q_c , taken from **Fig. 8a** increase from 0.91 in 0.3 M ZnO, 0.97 in 0.5 M ZnO and 0.98 in 0.7 M ZnO (**Table 3**). The lower charge ratio in 0.3 M ZnO can be attributed to increased parasitic HER. Increasing ZnO concentrations have been shown to reduce HER by Ravindran and Muralidharan [39] by decreasing water activity. Higher ZnO concentrations also facilitate more rapid zinc reduction and thus the competing HER is suppressed.

Nickel electrode charge ratios (Q_c/Q_a) also increase with ZnO concentration, from 0.95 in 0.3 M, 0.96 in 0.5 M, to 0.98 in 0.7 M ZnO. Cheng *et al.* [41] observed increased nickel electrode discharge capacities with the addition of ZnO to the electrolyte, attributing this to the intercalation of Zn^{2+} ions into the nickel hydroxide lattice, which acts as an additive to the

nickel electrode, preventing the conversion of β -NiO(OH) to γ -NiO(OH) and associated OER, improving coulombic efficiency and cycling stability. As shown in **Fig. 8c** and **8d**, coulombic efficiency in the zinc-nickel flow cell is limited by the discharge capacity of the nickel electrode, and demonstrates the same trend observed in charge ratios during cyclic voltammetry. Average coulombic efficiencies of 93.0 %, 94.7 % and 96.6 % are achieved in 0.3 M, 0.5 M and 0.7 M ZnO respectively.

4. Conclusions

TEAH and TEAB electrolyte additives have been examined in terms of their effect on zinc electrodeposition morphology and zinc-nickel flow cell performance. The best cycling performance is achieved with 15 mM TEAH, providing average coulombic and energy efficiencies of 98 % and 86 % respectively over 70 stable charge/discharge cycles. A smooth and compact zinc morphology is observed upon a final charge phase at the end of 80 cycles.

The results have shown that high concentrations of KOH inhibit zinc reduction by limiting the transport of Zn^{2+} to the electrode, while nickel electrode overpotentials are found to be reduced with increasing KOH concentrations due to the availability of OH^- for the nickel oxidation reaction. A 6 M concentration of KOH is preferred as it provides the highest coulombic efficiency during zinc-nickel flow cell cycling, displaying the highest conductivity at 293 K and maintaining reasonably low viscosity. Increasing ZnO electrolyte concentrations have been shown to be beneficial to coulombic efficiency at both the zinc and nickel electrodes and a zinc-nickel flow cell. Improved cycling performance is achieved in a 6 M KOH/0.5 M ZnO electrolyte and provided the highest average coulombic and voltaic efficiencies of 97.9 % and 87.8 % respectively and the consequent energy efficiency 86 %.

In order to obtain the optimum battery performance, it is essential to examine other influential factors, such as electrode substrate material, electrolyte flow rate, and current density, on Zn-Ni RFB system. We have been undertaking these related research and the findings will be communicated in later papers.

Acknowledgements

The authors would like to acknowledge the discussion and support received from Prof Nigel Brandon and his research group in Imperial College London, Mr John Collins and Dr David Hall in C-Tech Innovation Ltd, and Dr Ian Whyte in WhEST Ltd. Funding: This work was supported by the Engineering and Physical Sciences Research Council (EPSRC) Supergen Energy Storage Project (grant number: EP/P003494/1) entitled ‘Zinc-Nickel Redox Flow Battery for Energy Storage’; the EPSRC PhD studentship as a Doctoral Training Partnership (DTP); and the support from the College of Engineering, Mathematics and Physical Sciences in the University of Exeter.

References

- [1] P. Leung, X. Li, C. Ponce De León, L. Berlouis, C.T.J. Low, F.C. Walsh, Progress in redox flow batteries, remaining challenges and their applications in energy storage, *RSC Adv.* 2 (2012) 10125–10156. <https://doi.org/10.1039/c2ra21342g>.
- [2] M. Skyllas-Kazacos, M.H. Chakrabarti, S.A. Hajimolana, F.S. Mjalli, M. Saleem, Progress in Flow Battery Research and Development, *J. Electrochem. Soc.* 158 (2011) R55–%79. <https://doi.org/10.1149/1.3599565>.
- [3] P.K. Leung, C.P. De Leon, F.C. Walsh, The influence of operational parameters on the performance of an undivided zinc – cerium flow battery, *Electrochim. Acta.* 80 (2012) 7–14. <https://doi.org/10.1016/j.electacta.2012.06.074>.
- [4] L.F. Arenas, A. Loh, D.P. Trudgeon, X. Li, C. Ponce de León, F.C. Walsh, The characteristics and performance of hybrid redox flow batteries with zinc negative electrodes for energy storage, *Renew. Sustain. Energy Rev.* 90 (2018). <https://doi.org/10.1016/j.rser.2018.03.016>.
- [5] D.E. Turney, M. Shmukler, K. Galloway, M. Klein, Y. Ito, T. Sholkapper, J.W. Galloway, M. Nyce, S. Banerjee, Development and testing of an economic grid-scale flow-assisted zinc/nickel-hydroxide alkaline battery, *J. Power Sources.* 264 (2014) 49–58. <https://doi.org/10.1016/j.jpowsour.2014.04.067>.
- [6] A. Khor, P. Leung, M.R. Mohamed, C. Flox, Q. Xu, L. An, R.G.A. Wills, J.R. Morante, A.A. Shah, Review of zinc-based hybrid flow batteries: From fundamentals to applications, *Mater. Today Energy.* 8 (2018) 80–108. <https://doi.org/10.1016/j.mtener.2017.12.012>.
- [7] L.F. Arenas, A. Loh, D.P. Trudgeon, X. Li, C. Ponce de León, F.C. Walsh, The characteristics and performance of hybrid redox flow batteries with zinc negative electrodes for energy storage, *Renew. Sustain. Energy Rev.* 90 (2018) 992–1016. <https://doi.org/10.1016/j.rser.2018.03.016>.
- [8] J. McBreen, E. Gannon, The Electrochemistry of Metal Oxide Additives in Pasted Zinc Electrodes, *Electrochim. Acta.* 26 (1981) 1439–1446.
- [9] J. McBreen, M.G. Chu, G. Adzic, Substrate Effects on Zinc Deposition from Zincate Solutions: II. Deposition on Pb, Tl, Sn and In, *J. Electrochem. Soc.* 128 (1981) 2287–2292. <https://doi.org/10.1149/1.2127236>.
- [10] M.G. Chu, J. McBreen, G. Adzic, Substrate Effects on Zinc Deposition from Zincate Solutions: I. Deposition on Cu, Au, Cd and Zn, *J. Electrochem. Soc.* 128 (1981) 2281–2286.
- [11] G. Adzic, J. McBreen, M.G. Chu, Adsorption and Alloy Formation of Zinc Layers on Silver, *J. Electrochem. Soc.* 128 (1981) 1691–1697. <https://doi.org/10.1149/1.2127712>.
- [12] X. Wei, D. Desai, G.G. Yadav, D.E. Turney, A. Couzis, Impact of anode substrates on electrodeposited zinc over cycling in zinc-anode rechargeable alkaline batteries, *Electrochim. Acta.* 212 (2016) 603–613. <https://doi.org/10.1016/j.electacta.2016.07.041>.
- [13] L. Zhang, J. Cheng, Y. Yang, Y. Wen, X. Wang, G. Cao, Study of zinc electrodes for single flow zinc/nickel battery application, *J. Power Sources.* 179 (2008) 381–387.

- <https://doi.org/10.1016/j.jpowsour.2007.12.088>.
- [14] G. Nikiforidis, L. Berlouis, D. Hall, D. Hodgson, A study of different carbon composite materials for the negative half-cell reaction of the zinc cerium hybrid redox flow cell, *Electrochim. Acta.* 113 (2013) 412–423. <https://doi.org/10.1016/j.electacta.2013.09.061>.
- [15] G. Nikiforidis, L. Berlouis, D. Hall, D. Hodgson, Evaluation of carbon composite materials for the negative electrode in the zinc-cerium redox flow cell, *J. Power Sources.* 206 (2012) 497–503. <https://doi.org/10.1016/j.jpowsour.2011.01.036>.
- [16] Y. Cheng, H. Zhang, Q. Lai, X. Li, Q. Zheng, X. Xi, C. Ding, Effect of temperature on the performances and in situ polarization analysis of zinc–nickel single flow batteries, *J. Power Sources.* 249 (2014) 435–439. <https://doi.org/10.1016/j.jpowsour.2013.10.115>.
- [17] R.Y. Wang, D.W. Kirk, G.X. Zhang, Effects of Deposition Conditions on the Morphology of Zinc Deposits from Alkaline Zincate Solutions, *J. Electrochem. Soc.* 153 (2006) C357. <https://doi.org/10.1149/1.2186037>.
- [18] B. Sharifi, M. Mojtahedi, M. Goodarzi, J. Vahdati Khaki, Effect of alkaline electrolysis conditions on current efficiency and morphology of zinc powder, *Hydrometallurgy.* 99 (2009) 72–76. <https://doi.org/10.1016/j.hydromet.2009.07.003>.
- [19] W. Hong, Z. Jia, B. Wang, Influence of cathodic overpotential and zincate concentration on zinc deposition in alkaline solution :, *J. Appl. Electrochem.* 46 (2016) 1085–1090. <https://doi.org/10.1007/s10800-016-0990-9>.
- [20] Y. Cheng, X. Xi, D. Li, X. Li, Q. Lai, H. Zhang, Performance and potential problems of high power density zinc-nickel single flow batteries, *RSC Adv.* 5 (2015) 1772–1776. <https://doi.org/10.1039/c4ra12812e>.
- [21] K. Wang, P. Pei, Z. Ma, H. Xu, P. Li, X. Wang, Morphology control of zinc regeneration for zinc–air fuel cell and battery, *J. Power Sources.* 271 (2014) 65–75. <https://doi.org/10.1016/j.jpowsour.2014.07.182>.
- [22] R.D. Naybour, The Effect of Electrolyte Flow on the Morphology of Zinc Electrodeposited from Aqueous Alkaline Solution Containing Zincate Ions, *J. Electrochem. Soc.* 116 (1969) 520–524. <https://doi.org/10.1149/1.2411939>.
- [23] T. Otani, Y. Fukunaka, T. Homma, Effect of lead and tin additives on surface morphology evolution of electrodeposited zinc, *Electrochim. Acta.* 242 (2017) 364–372. <https://doi.org/10.1016/j.electacta.2017.04.130>.
- [24] T. Kakeya, A. Nakata, H. Arai, Z. Ogumi, Enhanced zinc electrode rechargeability in alkaline electrolytes containing hydrophilic organic materials with positive electrode compatibility, *J. Power Sources.* 407 (2018) 180–184. <https://doi.org/10.1016/j.jpowsour.2018.08.026>.
- [25] G.D. Wilcox, P.J. Mitchell, Electrolyte additives for zinc-anoded secondary cells I. Brighteners, levellers and complexants, *J. Power Sources.* 28 (1989) 345–359. [https://doi.org/10.1016/0378-7753\(89\)80064-3](https://doi.org/10.1016/0378-7753(89)80064-3).
- [26] G.D. Wilcox, P.J. Mitchell, Electrolyte additives for zinc-anoded secondary cells II. Quaternary ammonium compounds, *J. Power Sources.* 32 (1990) 31–41. [https://doi.org/10.1016/0378-7753\(90\)80031-8](https://doi.org/10.1016/0378-7753(90)80031-8).
- [27] J.C. Ballesteros, P. Diaz-Arista, Y. Meas, R. Ortega, G. Trejo, Zinc electrodeposition

- in the presence of polyethylene glycol 20000, *Electrochim. Acta.* 52 (2007) 3686–3696. <https://doi.org/10.1016/j.electacta.2006.10.042>.
- [28] J.M. Wang, L. Zhang, C. Zhang, J.Q. Zhang, Effects of bismuth ion and tetrabutylammonium bromide on the dendritic growth of zinc in alkaline zincate solutions, *J. Power Sources.* 102 (2001) 139–143. [https://doi.org/10.1016/S0378-7753\(01\)00789-3](https://doi.org/10.1016/S0378-7753(01)00789-3).
- [29] C.J. Lan, C.Y. Lee, T.S. Chin, Tetra-alkyl ammonium hydroxides as inhibitors of Zn dendrite in Zn-based secondary batteries, *Electrochim. Acta.* 52 (2007) 5407–5416. <https://doi.org/10.1016/j.electacta.2007.02.063>.
- [30] J. Zhu, Y. Zhou, C. Gao, Influence of surfactants on electrochemical behavior of zinc electrodes in alkaline solution, *J. Power Sources.* 72 (1998) 231–235. [https://doi.org/10.1016/S0378-7753\(97\)02705-5](https://doi.org/10.1016/S0378-7753(97)02705-5).
- [31] P.K. Leung, C. Ponce-De-León, C.T.J. Low, F.C. Walsh, Zinc deposition and dissolution in methanesulfonic acid onto a carbon composite electrode as the negative electrode reactions in a hybrid redox flow battery, *Electrochim. Acta.* 56 (2011) 6536–6546. <https://doi.org/10.1016/j.electacta.2011.04.111>.
- [32] J.W. Diggle, A. Damjanovic, The Inhibition of the Dendritic Electrocrystallization of Zinc from Doped Alkaline Zincate Solutions, *J. Electrochem. Soc.* 119 (1972) 1649–1658.
- [33] J.L. Ortiz-Aparicio, Y. Meas, T.W. Chapman, G. Trejo, R. Ortega, E. Chainet, Electrodeposition of zinc in the presence of quaternary ammonium compounds from alkaline chloride bath, *J. Appl. Electrochem.* 45 (2015) 67–78. <https://doi.org/10.1007/s10800-014-0777-9>.
- [34] F. Mansfeld, S. Gilman, The Effect of Tin and Tetraethylammonium Ions on the Characteristics of Zinc Deposition on a Zinc Single Crystal in Aqueous KOH, *J. Electrochem. Soc.* 117 (1970) 1154–1155. <https://doi.org/10.1149/1.2407757>.
- [35] Y. Wen, T. Wang, J. Cheng, J. Pan, G. Cao, Y. Yang, Lead ion and tetrabutylammonium bromide as inhibitors of the growth of spongy zinc in single flow zinc/nickel batteries, *Electrochim. Acta.* 59 (2012) 64–68. <https://doi.org/10.1016/j.electacta.2011.10.042>.
- [36] D.P. Trudgeon, K. Qiu, X. Li, T. Mallick, O.O. Taiwo, B. Chakrabarti, V. Yufit, N.P. Brandon, D. Crevillen-Garcia, A. Shah, Screening of effective electrolyte additives for zinc-based redox flow battery systems, *J. Power Sources.* 412 (2019) 44–54. <https://doi.org/10.1016/j.jpowsour.2018.11.030>.
- [37] A.R. Mainar, O. Leonet, M. Bengoechea, I. Boyano, I. de Meatza, A. Kvasa, A. Guerfi, J.A. Blazquez, Alkaline aqueous electrolytes for secondary zinc-air batteries: an overview, *Int. J. Energy Res.* 40 (2016) 1032–1049. <https://doi.org/10.1002/er.3499>.
- [38] P. Sapkota, H. Kim, An experimental study on the performance of a zinc air fuel cell with inexpensive metal oxide catalysts and porous organic polymer separators, *J. Ind. Eng. Chem.* 16 (2010) 39–44. <https://doi.org/10.1016/j.jiec.2010.01.024>.
- [39] V. Ravindran, V.S. Muralidharan, Cathodic processes on zinc in alkaline zincate solutions, *J. Power Sources.* 55 (1995) 237–241. [https://doi.org/10.1016/0378-7753\(95\)02184-I](https://doi.org/10.1016/0378-7753(95)02184-I).
- [40] H. Vaidyanathan, K. Robbins, G.M. Rao, Effect of KOH concentration and anions on

- the performance of a Ni-H₂ battery positive plate, *J. Power Sources*. 63 (1996) 7–13. [https://doi.org/10.1016/S0378-7753\(96\)02435-4](https://doi.org/10.1016/S0378-7753(96)02435-4).
- [41] J. Cheng, Y.-H. Wen, G.-P. Cao, Y.-S. Yang, Influence of zinc ions in electrolytes on the stability of nickel oxide electrodes for single flow zinc–nickel batteries, *J. Power Sources*. 196 (2011) 1589–1592. <https://doi.org/http://dx.doi.org/10.1016/j.jpowsour.2010.08.009>.
- [42] F.C. Anson, Innovations in the Study of Adsorbed Reactants by Chronocoulometry, *Anal. Chem.* 38 (1966) 54–57. <https://doi.org/10.1021/ac60233a014>.
- [43] M. Schlesinger, M. Paunovic, Fundamental Considerations, in: *Mod. Electroplat.*, 4th ed., John Wiley & Sons Inc., New York, 2000: pp. 1–32.
- [44] R.J. Gilliam, J.W. Graydon, D.W. Kirk, S.J. Thorpe, A review of specific conductivities of potassium hydroxide solutions for various concentrations and temperatures, *Int. J. Hydrogen Energy*. 32 (2007) 359–364. <https://doi.org/10.1016/j.ijhydene.2006.10.062>.
- [45] F. Allebrod, C. Chatzichristodoulou, P.L. Mollerup, M.B. Mogensen, Electrical conductivity measurements of aqueous and immobilized potassium hydroxide, *Int. J. Hydrogen Energy*. 37 (2012) 16505–16514. <https://doi.org/10.1016/j.ijhydene.2012.02.088>.
- [46] M.B. Liu, G.M. Cook, N.P. Yao, B.R. Faulds, Conductivity of KOH Electrolyte Supersaturated with Zincate, *J. Electrochem. Soc.* 128 (1981) 2049–2052. <https://doi.org/10.1149/1.2127187>.
- [47] W.H. Dyson, L.A. Schreier, Physical-Chemical Studies of KOH-ZnO Electrolytes, *J. Electrochem. Soc.* 115 (1968) 566–569.
- [48] S. Siu, J.W. Evans, Density and viscosity measurements of zincate/KOH solutions, *J. Electrochem. Soc.* 144 (1997) 1278–1280. <https://doi.org/10.1149/1.1837583>.
- [49] D. Pletcher, Techniques for the Study of Electrode Reactions, in: *A First Course Electrode Process.*, 2nd ed., RSC Publishing, Cambridge, 2009: p. 206.
- [50] J.O. Bockris, Z. Nagy, A. Damjanovic, On the Deposition and Dissolution of Zinc in Alkaline Solutions, *J. Electrochem. Soc.* 119 (1972) 285. <https://doi.org/10.1149/1.2404188>.
- [51] J. Hendrikx, A. Van Der Putten, W. Visscher, E. Barendrecht, The electrodeposition and dissolution of zinc and amalgamated zinc in alkaline solutions, *Electrochim. Acta*. 29 (1984) 81–89.
- [52] D. Pletcher, An Introduction to Electrode Reactions, in: *A First Course Electrode Process.*, 2nd ed., RSC Publishing, Cambridge, 2009: p. 45.
- [53] L.Ž. Vorkapić, D.M. Dražić, A.R. Despić, Corrosion of Pure and Amalgamated Zinc in Concentrated Alkali Hydroxide Solutions, *J. Electrochem. Soc.* 121 (2007) 1385. <https://doi.org/10.1149/1.2401695>.
- [54] E. Budevski, G. Staikov, W.J. Lorenz, Electrocrystallization: Nucleation and growth phenomena, *Electrochim. Acta*. 45 (2000) 2559–2574. [https://doi.org/10.1016/S0013-4686\(00\)00353-4](https://doi.org/10.1016/S0013-4686(00)00353-4).

Table 1: Zinc reduction onset potentials, anodic/cathodic peak separation, anodic/cathodic charge ratio data taken from cyclic voltammograms (Fig. 1a and b). Anodic/cathodic charge ratios are averaged over 5 stable cycles from 2 CV tests. Current ranges taken from results of chronoamperometry (Fig. 2a and b). Estimated surface area of zinc deposits calculated from Anson plots (Fig. 2c and d).

Additive	Zinc reduction onset potential, E_R, V vs. Hg/HgO	Anodic/cathodic peak separation, ΔE_p, mV	Anodic/cathodic charge ratio, Q_a/Q_c	Current range during 60 minute deposition, mA	Estimated Surface Area of Zinc Deposited, cm²	Coefficients of Determination, R²
No Additive	-1.390	205	0.82	201	25.7	0.988
1 mM TEAH	-1.391	216	0.86	127	23.4	0.983
5 mM TEAH	-1.402	226	0.90	100	20.7	0.988
10 mM TEAH	-1.403	240	0.94	63	16.7	0.989
15 mM TEAH	-1.417	255	0.96	62	15.9	0.988
20 mM TEAH	-1.428	267	0.96	43	16.7	0.990
1 mM TEAB	-1.397	207	0.86	210	22.5	0.984
5 mM TEAB	-1.416	250	0.91	86	19.5	0.988
10 mM TEAB	-1.430	260	0.94	78	18.8	0.986
15 mM TEAB	-1.431	261	0.96	62	15.9	0.983
20 mM TEAB	-1.438	267	0.96	53	16.3	0.993

Table 2: Average electrode potentials, coulombic, voltaic and energy efficiencies over 70 charge/discharge cycles in an electrolyte solution of 6 M KOH + 0.5 M ZnO with no additive and with TEAH and TEAB additives at varying concentrations.

Additive	Average Electrode Potential vs. Hg/HgO, V				Average Efficiencies, %		
	Charge		Discharge		Coulombic	Voltaic	Energy
	Zinc	Nickel	Zinc	Nickel			
No Additive	-1.410	0.486	-1.360	0.338	95.2	89.6	85.2
5 mM TEAH	-1.423	0.485	-1.358	0.337	95.9	88.8	85.2
10 mM TEAH	-1.428	0.484	-1.345	0.340	96.7	88.2	85.3
15 mM TEAH	-1.437	0.484	-1.350	0.339	97.8	87.9	86.0
20 mM TEAH	-1.446	0.485	-1.346	0.339	89.3	87.3	78.0
5 mM TEAB	-1.424	0.483	-1.359	0.338	96.2	88.9	85.5
10 mM TEAB	-1.427	0.486	-1.348	0.338	96.8	88.1	85.3
15 mM TEAB	-1.437	0.483	-1.347	0.339	97.3	87.8	85.4
20 mM TEAB	-1.437	0.487	-1.343	0.342	92.0	87.6	80.6

Table 3: Results of cyclic voltammetry and zinc-nickel flow cell cycling. Properties of electrolytes under investigation. Measurements made at 293 K

Concentration, mol L ⁻¹		Cyclic voltammetry - zinc electrode		Cyclic voltammetry - nickel electrode		Zinc-nickel flow cell cycling			Conductivity, mS cm ⁻²	Kinematic viscosity, mm ² s ⁻¹	Density, g mL ⁻¹	Dynamic Viscosity, mPa s ⁻¹
KOH	ZnO	Charge balance, Q_a/Q_c	E_c , V vs. Hg/HgO	Charge balance, Q_c/Q_a	$E_{j=0}$, V vs. Hg/HgO	Voltaic efficiency, %	Coulombic efficiency, %	Energy efficiency, %				
4	0.3	0.88	-1.354	0.95	0.307	85.3	92.8	79.2	423	1.462	1.219	1.782
6	0.3	0.91	-1.398	0.97	0.284	85.4	97.5	83.3	501	1.831	1.297	2.375
8	0.3	0.91	-1.411	0.95	0.251	83.0	93.0	77.2	464	2.361	1.368	3.231
8	0.5	0.97	-1.409	0.96	0.255	83.0	94.7	78.6	450	2.421	1.382	3.345
8	0.7	0.98	-1.406	0.98	0.252	83.1	96.6	80.3	435	2.608	1.405	3.664

Figure Captions

Fig. 1 Cyclic voltammograms obtained from electrolyte solutions containing: (a) TEAH and (b) TEAB additives in a base electrolyte of 6 M KOH/0.6 M ZnO. Potential sweep rate 20 mV s⁻¹.

Fig. 2 Current responses obtained at -1.6 V vs. Hg/HgO in electrolyte solutions containing: (a) TEAH and (b) TEAB in a 6 M KOH/0.5 M ZnO base electrolyte. Anson plots obtained at a potential of -1.6 V vs. Hg/HgO on zinc depositions until the charge passed reached 36 C/10 mA h, (c) TEAH, (d) TEAB.

Fig. 3 Coulombic efficiencies as a function of cycle number for a zinc-nickel flow cell during 80 charge/discharge cycles in an electrolyte solution of 6 M KOH + 0.5 M ZnO with no additive and with (a) TEAH and (b) TEAB additives.

Fig. 4 Potential responses for a zinc-nickel flow cell during 30 charge/discharge cycles in an electrolyte solution of 6 M KOH + 0.5 M ZnO with no additive: (a) nickel electrode. (b) zinc electrode.

Fig. 5 SEM images of zinc deposits obtained after 80 charge/discharge cycles from electrolyte solutions containing 6 M KOH + 0.5 M ZnO with varying concentrations of TEAH: (a) No additive, (b) 5 mM TEAH, (c) 10 mM TEAH, (d) 15 mM TEAH, (e) 20 mM TEAH. SEM magnifications: 100 (inset magnifications: 25 k).

Fig. 6 Visualisation of zinc electrodeposition in the presence of: (a) a moderate additive concentration and (b) an excessive additive concentration.

Fig. 7 Cyclic voltammograms obtained in electrolyte solutions containing 0.3 M ZnO, 15 mM TEAH and varying KOH concentrations: (a) at zinc electrode (BMA5 substrate); (b) at sintered nickel electrode. Potential sweep rate 10 mV s⁻¹. Charge/discharge curves for the 50th cycle in electrolyte solutions containing 0.3 M ZnO, 15 mM TEAH and varying KOH concentrations: (a) at zinc electrode, (b) at nickel electrode.

Fig. 8 Cyclic voltammograms obtained in electrolyte solutions containing 8 M KOH, 15 mM TEAH and varying ZnO concentrations: (a) at zinc electrode (BMA5 substrate); (b) at sintered nickel electrode. Potential sweep rate 10 mV s^{-1} . Charge/discharge curves for the 50th cycle in electrolyte solutions containing 8 M KOH, 15 mM TEAH and varying ZnO concentrations: (a) at zinc electrode, (b) at nickel electrode.

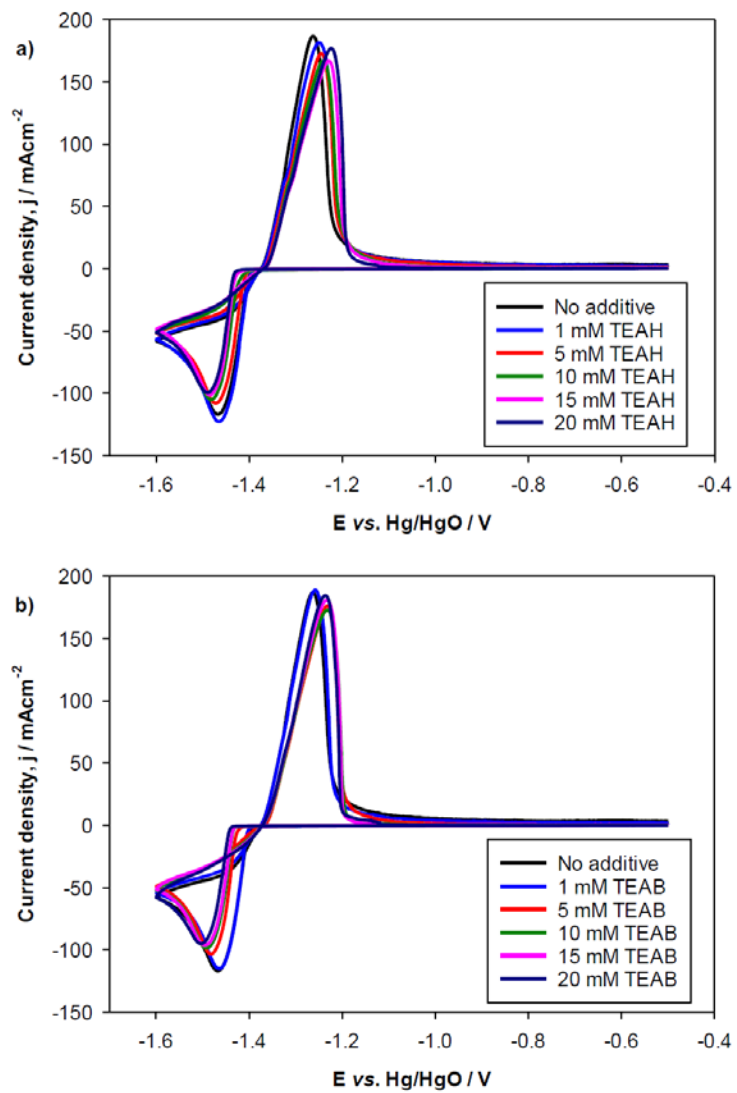


Fig. 1

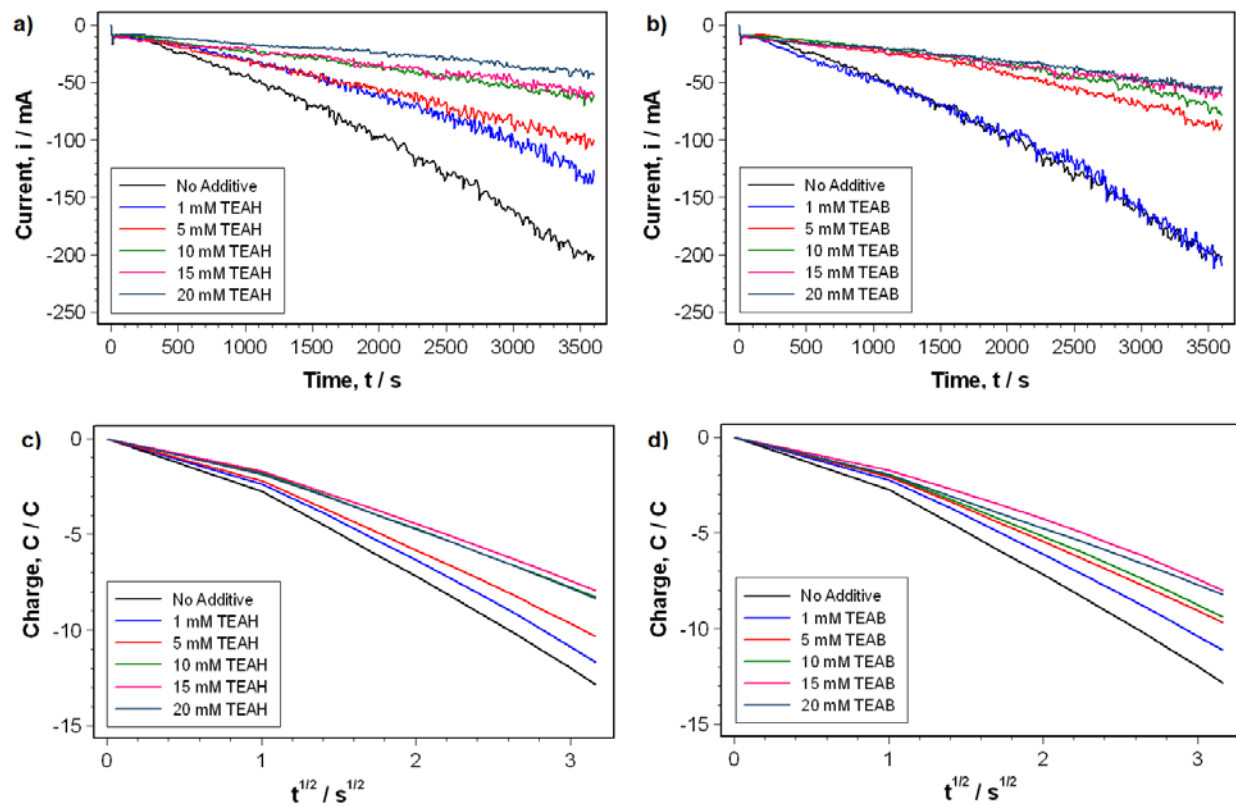


Fig. 2

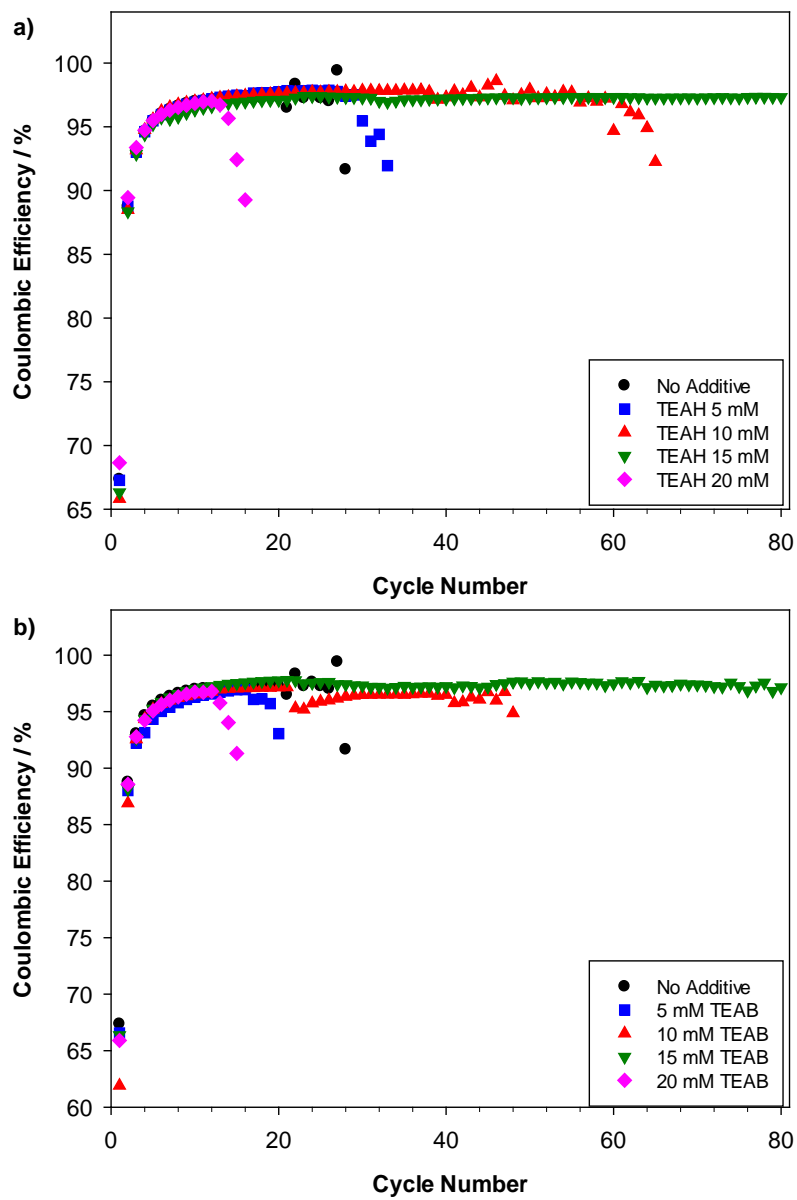


Fig. 3

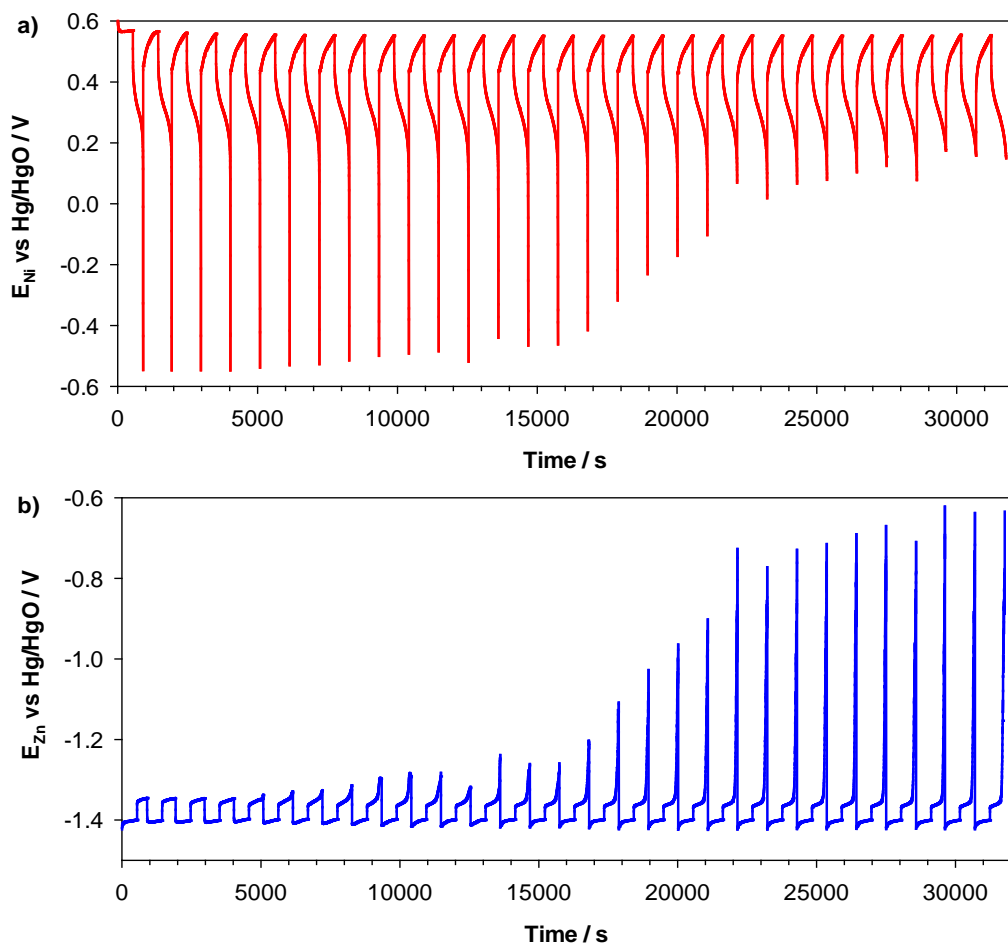


Fig. 4

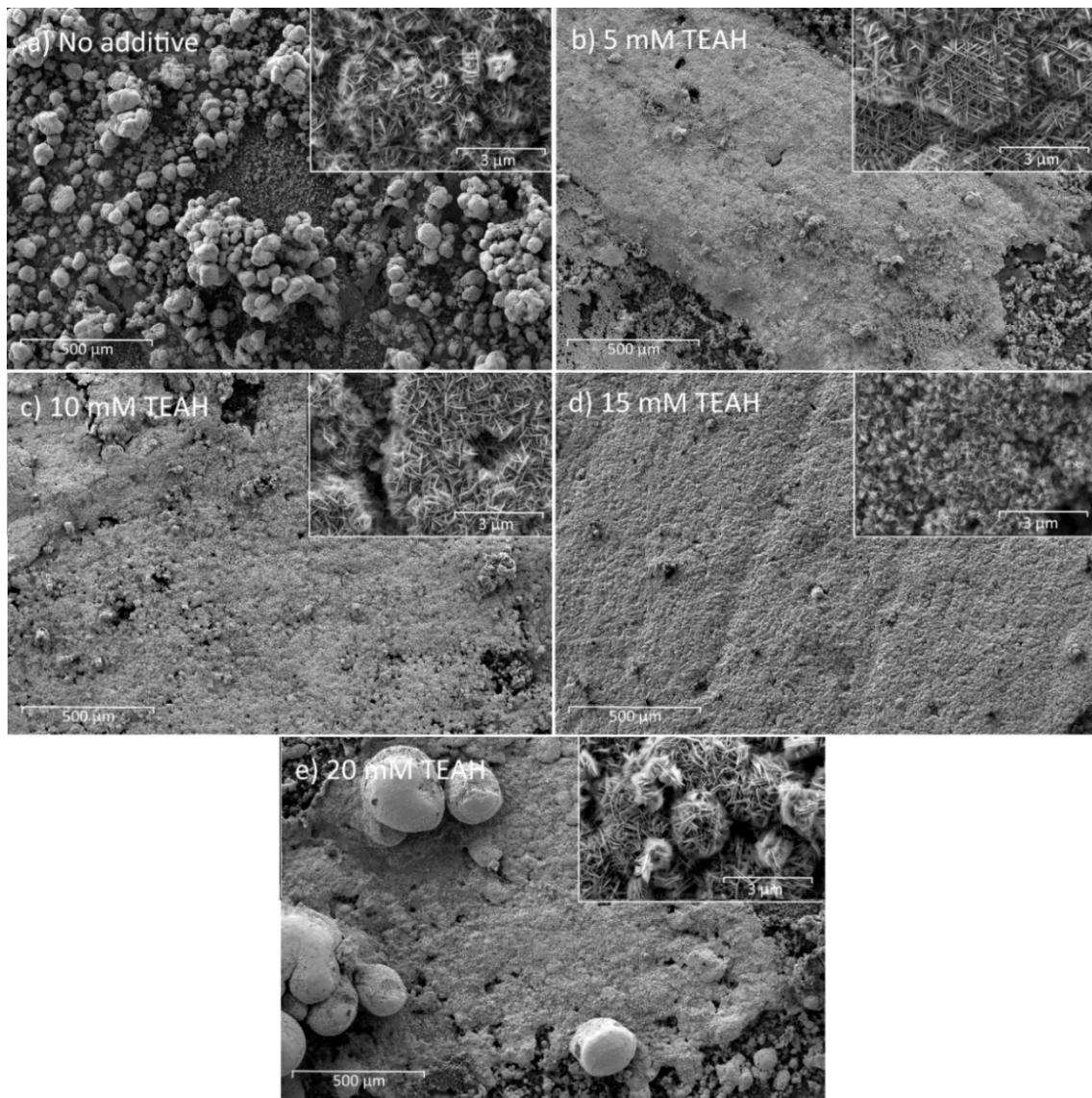


Fig. 5

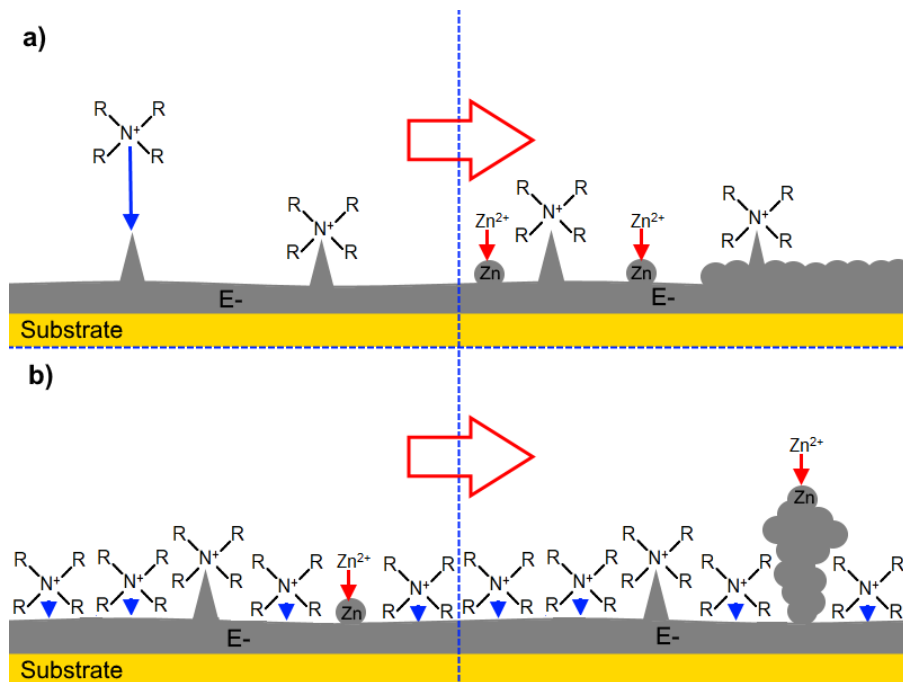


Fig. 6

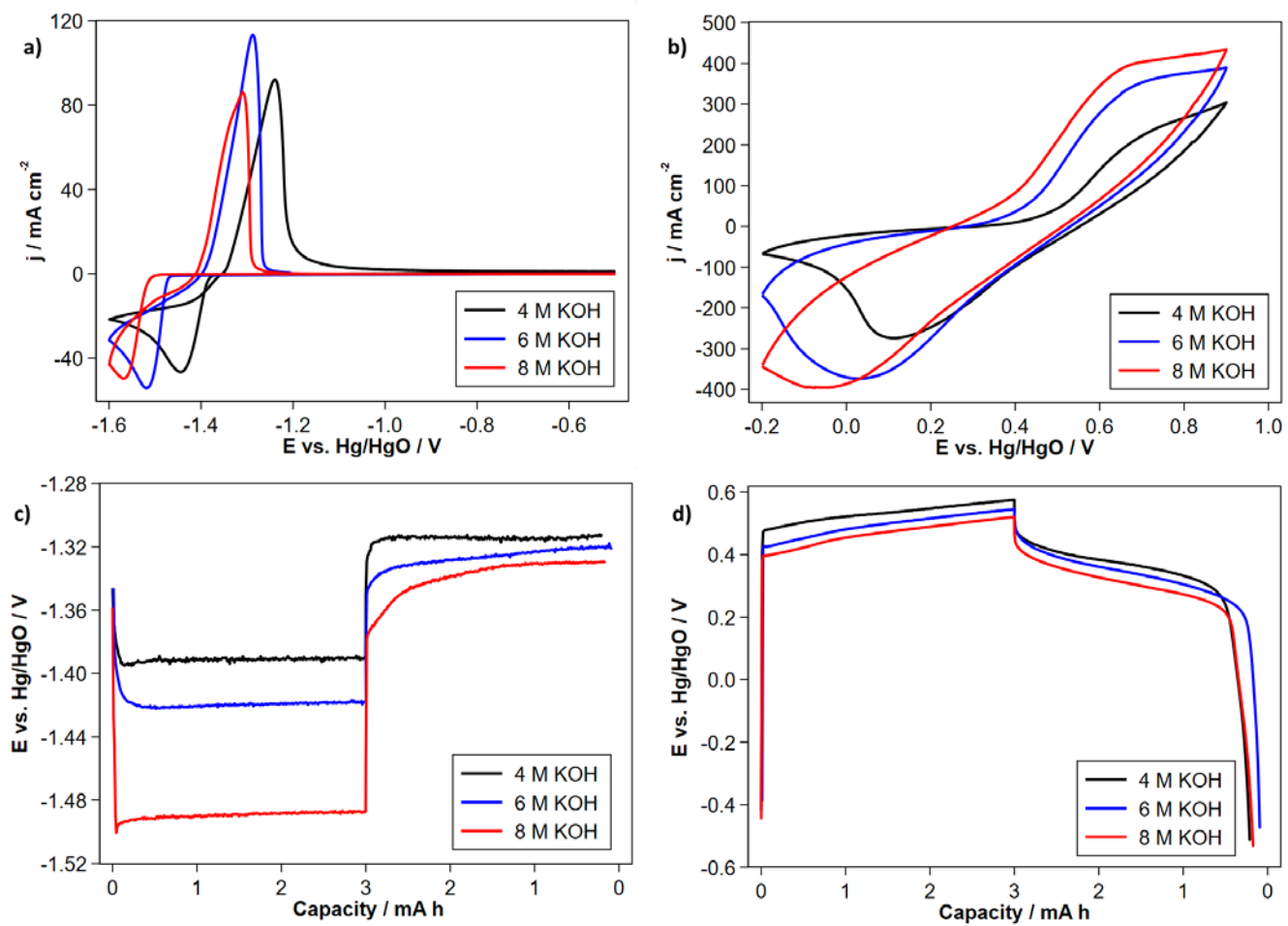


Fig. 7

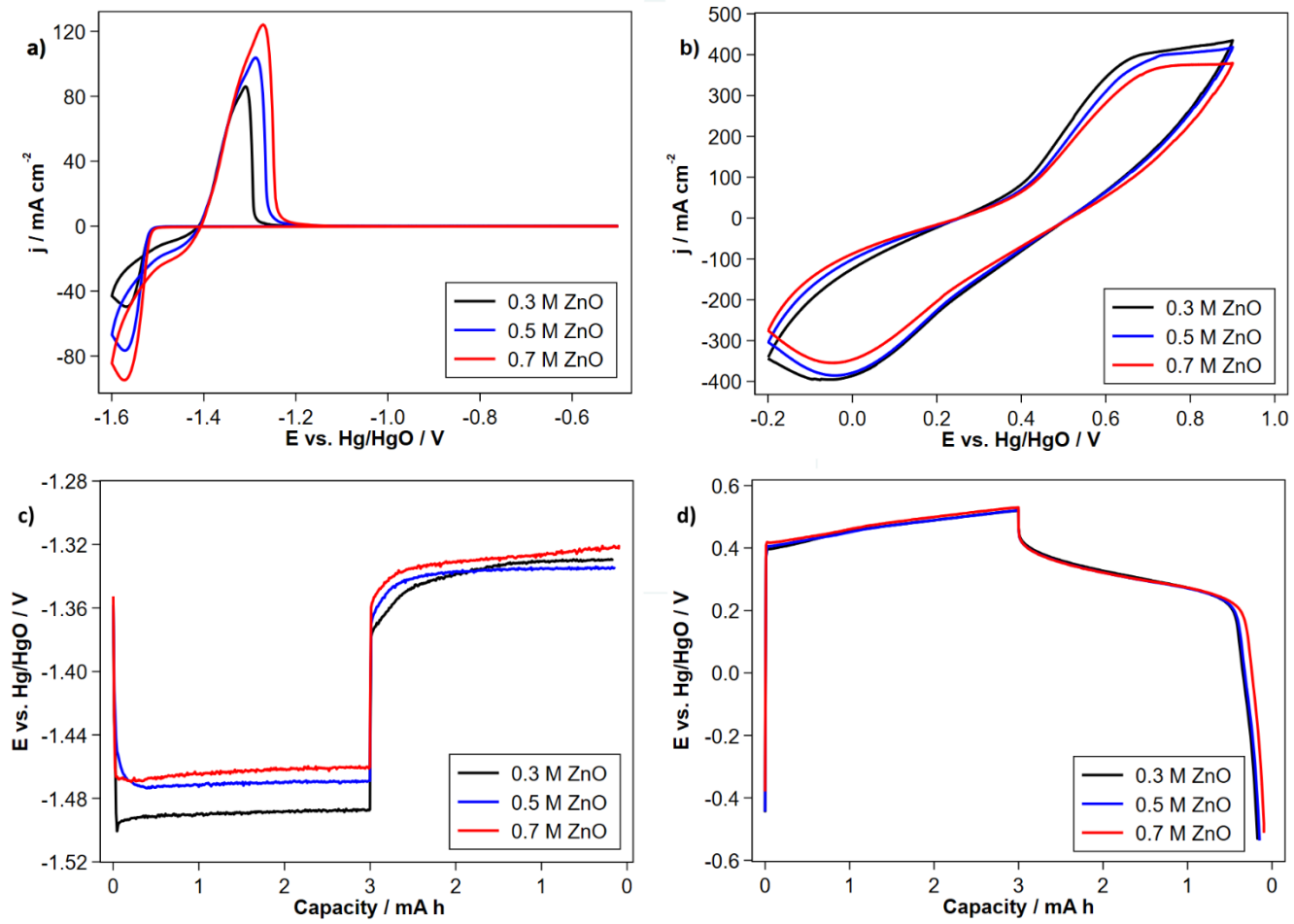


Fig. 8